Defect engineering using microwave processing in SiC and GaAs

Oleg Olikh[1]‡**, Petro Lytvyn**[2]

[1]Physics Faculty, Taras Shevchenko National University of Kyiv, Kyiv 01601, Ukraine
[2]V. Lashkaryov Institute of Semiconductor Physics of NAS of Ukraine, Kyiv 03028, Ukraine

E-mail: `olegolikh@knu.ua`

Abstract. The influence of microwave radiation (2.45 GHz, 1.5 W/cm^2, up to 80 s) on defects was studied in single crystals of n-6H–SiC, n-GaAs, and epi-GaAs. The capture cross section of the charge carrier was found to change, and defect complexes were reconstructed because of the growing number of interstitial atoms in the near-surface layer. The correlation between the changes in the defect subsystem and deformation of the near-surface layer was analyzed. The possible mechanisms of the revealed effects are also discussed.

‡ Author to whom any correspondence should be addressed.

1. Introduction

Microelectronics is currently a field of primary importance, and the investigation of how semiconductors and their structural properties change under the action of various external factors has become one of the most important tasks in material science. Numerous theoretical and experimental studies have aimed to reveal the degradation mechanisms of semiconductor structures and to develop new technologies for microelectronic devices improvement. The influence of certain factors, for example, radiation, has been studied quite well — see, for instance, [1, 2, 3]. At the same time, new agents begin to attract more attention, such as ultrasound loading (USL) [4, 5], or microwave treatment (MWT) [6, 7, 8, 9, 10, 11, 12, 13, 14, 15, 16, 17, 18, 19]. The MWT has been widely applied owing to its capability of heating solid bodies [6, 7]. This approach is unique because of its high efficiency and capability to increase the temperature of a sample as a whole or at selected locations with extremely high heating speeds [6]. As a result, MWT is widely used to synthesize various materials, and semiconductor compounds including [6, 8]. However, this type of external influence also causes changes in the characteristics of semiconductor materials and device structures. For instance, it has been found that irradiation by superhigh-frequency electromagnetic waves causes relaxation of internal stresses and modification of near-surface regions in GaAs and InP structures [11, 10, 12, 13, 15, 18, 19], leveling of surface microrelief in SiC/SiO_2 structures [9], redistribution of impurities [9, 16, 18], re-charge of complexes [12] and generation of defects [16]. The microwave-induced restructuring of impurity defects leads to a decrease in the spread of the Schottky diode parameters [12, 16]. Moreover, MWT has been found to induce changes in the properties of Ti, Gd, and Er films deposited on silicon carbide [17], as well as in the reconstruction of GaAs photoluminescence spectra [13, 15, 16], and the effect depends on both the type of dopant and the crystal structure orientation of the samples. Overall, these facts allow us to consider the MWT as one of the most promising ways to modify semiconductor devices.

However, it is well known that the properties of semiconductor structures are significally influenced by their defect subsystem. Defects in SiC and GaAs have been investigated extensively [20, 21, 22, 23]. At the same time, more detailed information regarding the MWT influence on the deep level parameters is practically unknown. The aim of this study was to investigate the impact of MWT on the defects located in the near-surface region of n–6H–SiC and n–GaAs single crystals, and GaAs epitaxial structures. The acoustoelectric transient spectroscopy was used to characterize the deep levels.
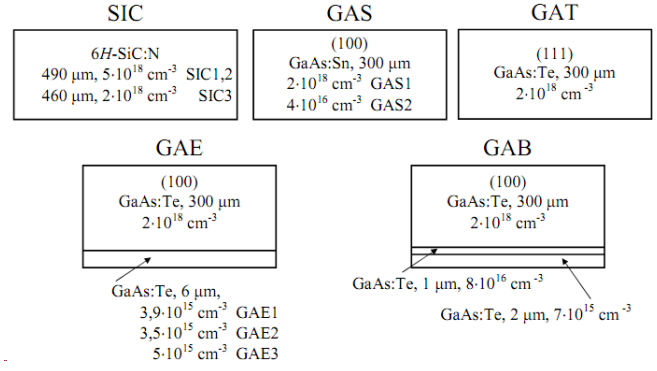

Figure 1. Schematic structure of the samples for deep level investigations

2. Experimental details

It has been reported [11, 12, 13, 14, 15] that the impact of MWT on semiconductor structures depends on many factors. The primary factors are the initial level of structural perfectness, conductivity, dielectric permittivity, and structural topology. To estimate the effect of MWT on the defect parameters, we selected different samples based on the doping degree, initial level of residual mechanical stress, and structure. They were as follows.

i) Single-crystal n–6H–SiC wafers were grown using the Leli method and were doped with nitrogen. The samples were 490 μm-thick plates with dimensions of 5×10 mm^2 and carrier concentration $n = (3 - 6) \times 10^{18}$ cm^{-3} (further on SIC1 and SIC2); and 460 μm thick wafers with the same dimensions and $n = (1 - 3) \times 10^{18}$ cm^{-3} (SIC3).

ii) Single-crystal GaAs wafers with a thickness of 300 μm. The [100] wafers were doped with tin, and the concentration of electrons was $(1.5 - 2.5) \times 10^{18}$ cm^{-3} for sample GAS1 and $(3 - 5) \times 10^{16}$ cm^{-3} for sample GAS2. GAT denotation is used for [111] wafer, which was doped with tellurium, $n = (1 - 2) \times 10^{18}$ cm^{-3}.

iii) Epitaxial n-n^+ structures of GaAs which were 300 μm thick single crystal substrates $n = 2 \times 10^{18}$ cm^{-3} covered with 6 μm thick layer with carrier concentration 3.9×10^{15} cm^{-3} (sample GAE1), 3.5×10^{15} cm^{-3} (GAE2), 5.0×10^{15} cm^{-3} (GAE3). The substrate and epitaxial layers were doped with Te.

iv) Epitaxial n-n^+-n^{++} structures of GaAs:Te with a buffer layer. They were made from a single-crystal (100) substrate (300 μm, $n = 2 \times 10^{18}$ cm^{-3}) subsequently covered with a 1 μm layer with $n = 8 \times 10^{16}$ cm^{-3} and a 2 μm layer with $n = 7 \times 10^{15}$ cm^{-3}. Two samples (GAB1 and GAB2) were cut from different wafers.

Epitaxial systems have been produced by using gas-phase epitaxy. The schematic structure of the samples under study are shown in figure 1.
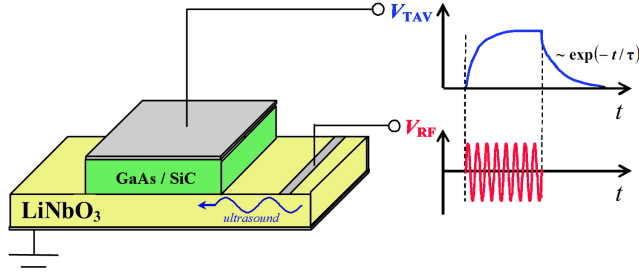
Figure 2. Scheme of TAV signal measurements. Time dependence of radio impulse V_{RF} of ultrasound excitation in piezoelectric plate and the resulting TAV signal V_{TAV} are shown schematically

The MWTs of the samples were performed in free space at room temperature in a magnetron at a frequency of $\nu = 2.45$ GHz and specific power of 1.5 W/cm^2. The epitaxial structures were irradiated onto the side of the epitaxial layer. The total exposure time t_{MWT} varied in the range of $20-80$ s for the different samples. To avoid essential heating, the maximum single irradiation exposure time was no more than five seconds.

The parameters of defects, such as the capture cross section of electron σ_n and the energy level with respect to the conductivity band bottom ($E_c - E_t$) were determined both before and after MWT. For this purpose, we used acoustoelectric transient spectroscopy [24, 25, 27, 26]. The principle of this spectroscopy closely coincides with the idea of the DLTS technique [28], but the barrier formation is not required, and defects at the epi-structure interface can be detected [24, 25, 27]. A schematic representation of method is shown in figure 2. The samples were placed on a LiNbO$_3$ piezoelectric plate in which acoustic waves were excited as impulses. After ultrasound impulse termination, relaxation of the transverse acoustoelectric voltage (TAV) occurs according to

$$V_{TAV}(t) = V_{TAV,0} \exp(-t/\tau). \tag{1}$$

A simple exponential dependence according to equation (1) is observed in cases where only one type of trap is effective in acoustoelectric interactions. For n-type semiconductors, the characteristic relaxation time is described by the equation [24, 27]

$$\tau = \frac{1}{\sigma_n\, v_{\mathrm{th},n}\, N_c} \exp\left(\frac{E_c - E_t}{kT}\right), \tag{2}$$

where $v_{\mathrm{th},n}$ is the electron thermal velocity and N_c is the density of states in the conduction band.

The experimental measurements of the TAV relaxation at different temperatures and further approximation according to equation (1) allowed us to obtain the $\tau(T)$ dependence. ($E_c - E_t$) was determined from the slope of τ dependence on $(kT)^{-1}$ in semilogarithmic scale and then, using equation (2), σ_n was

calculated. The measurements were performed in the temperature range $(290 - 350)$ K except for the GAB samples, the TAV for which was high enough to be measured only after heating to above 310 K.

For single–crystal samples before and after MWT, we also determined the curvature radius R_{cur} and deformation ξ_{cur} of the near-surface crystallographic planes. The value of ξ_{cur} was estimated by the X-ray method from the change in the angle of the diffraction maximum location during sample translation [29], and the curvature was measured using a profilometer DekTak 3030 Veeco Instruments. R_{cur} and ξ_{cur} were measured with a relative error no more than 2%. For GaAs single crystals, we also analyzed the distribution of structural defects over the area by using the Borman X-ray projection topography method, and estimated the distribution of dislocation densities and microstresses from the analysis of the intensities of the Friedel reflection pairs hkl and $hk\bar{l}$.

3. Results and discussion

Figure 3 presents the typical temperature dependencies of τ for the samples before and after the MWT. The above data show the MWT-induced change not only in the curve slopes (which is related to the level location in the gap), but also in the absolute value of the characteristic time of the TAV relaxation. The MWT impact depends not only on the exposure time and doping level but also on the internal structure of the samples under study. The summary of the trap parameters detected in the samples is presented in table 1. In the silicon carbide samples, there are two deep levels, labeled ESC1 and ESC2, while in gallium arsenide, there are six (EGA1–EGA6).

The presented results have several features:
i) The capture cross section is much more sensitive to the MWT influence than the level energy. For example, σ_n was found to change by an order of magnitude when the level shift was no more than 20%; besides, the lower exposition time was needed to change the capture cross-section. For instance, the ($E_c - E_t$) in GAB1 practically did not change after 20 s of MW exposure, whereas σ_n grew approximately four times.
ii) In single crystals, the MW-induced changes become stronger with a decrease in free charge carrier concentration (see GAS1 and GAS2 data) and an increase in the relative deformation (the surface curvature).
iii) The durable MWT of single-crystal samples ($t_{\mathrm{MWT}} > 40$ s for GaAs, $t_{\mathrm{MWT}} > 80$ s for SiC) leads to an essential decrease in TAV signal magnitude. This fact correlates with the data from [16], who reported a decrease in the concentration of centers with levels in the upper half of the band gap as a result of MW
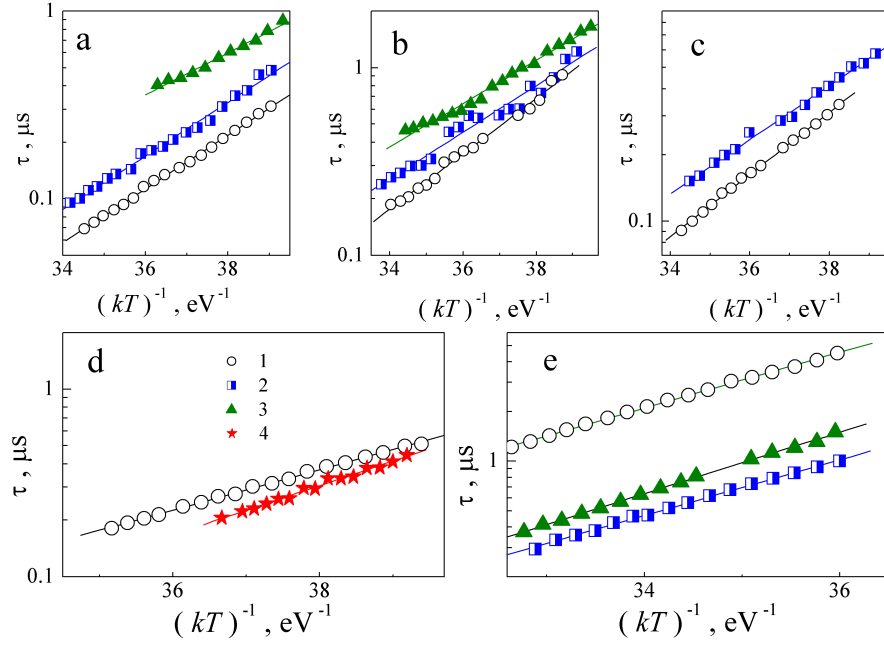
Figure 3. Dependencies of TAV relaxation time on inverse temperature for samples SIC2 (a), SIC3 (b), GAS2 (c), GAE2 (d) and GAB1 (e) before and after MWT. t_{MWT}, s: 0 (curves 1), 20 (2), 40 (3), 60 (4)

Table 1. The determined defect parameters in samples n–GaAs and n–$6H$–SiC

Sample	t_{MWT}, s	Level	$(E_c - E_t)$, eV	σ_n, cm^2 [a]	R_{cur}, m	ξ_{cur}
SIC1	0	ESC1	0.33 ± 0.01	$(7 \pm 4) \times 10^{-18}$	∞	0
	20	ESC1	0.33 ± 0.01	$(5 \pm 3) \times 10^{-19}$	170.2	8.7×10^{-7}
	40	ESC2	0.26 ± 0.01	$(2 \pm 1) \times 10^{-19}$		
	80		weak signal		-	
SIC2	0	ESC1	0.33 ± 0.01	$(7 \pm 4) \times 10^{-18}$	> 2000	$< 1.2 \times 10^{-7}$
	20	ESC1	0.33 ± 0.01	$(5 \pm 3) \times 10^{-19}$	171.9	1.4×10^{-6}
SIC3	0	ESC1	0.34 ± 0.02	$(3 \pm 2) \times 10^{-18}$	3.8	6.1×10^{-5}
	20	ESC2	0.29 ± 0.01	$(5 \pm 3) \times 10^{-19}$	5.5	4.2×10^{-5}
	40	ESC2	0.26 ± 0.01	$(10 \pm 7) \times 10^{-20}$		
	80	ESC2	0.23 ± 0.01	$(6 \pm 4) \times 10^{-20}$	-	
GAS1	0	EGA1	0.32 ± 0.02	$(3 \pm 2) \times 10^{-17}$	-53.8	-2.8×10^{-6}
	20	EGA1	0.31 ± 0.01	$(2 \pm 1) \times 10^{-17}$	22.9	6.5×10^{-6}
	40		weak signal		-	
GAS2	0	EGA1	0.32 ± 0.01	$(4 \pm 2) \times 10^{-17}$	17.2	8.7×10^{-6}
	20	EGA2	0.28 ± 0.01	$(5 \pm 2) \times 10^{-18}$	14.7	1.0×10^{-5}
	40		weak signal		-	
GAT	0	EGA3	0.49 ± 0.02	$(5 \pm 3) \times 10^{-14}$		
	20	EGA4	0.40 ± 0.02	$(2 \pm 1) \times 10^{-15}$		
GAE1	0	EGA5	0.24 ± 0.01	$(2 \pm 1) \times 10^{-18}$		
	60	EGA2	0.29 ± 0.01	$(10 \pm 6) \times 10^{-18}$		
GAE2	0	EGA5	0.25 ± 0.01	$(2 \pm 1) \times 10^{-18}$		
	60	EGA2	0.30 ± 0.01	$(2 \pm 1) \times 10^{-17}$		
GAE3	0	EGA6	0.43 ± 0.01	$(8 \pm 5) \times 10^{-17}$		
	60	EGA6	0.46 ± 0.02	$(7 \pm 4) \times 10^{-16}$	-	
GAB1	0	EGA4	0.39 ± 0.01	$(10 \pm 7) \times 10^{-18}$		
	20	EGA4	0.39 ± 0.01	$(4 \pm 2) \times 10^{-17}$		
	40	EGA6	0.43 ± 0.02	$(10 \pm 6) \times 10^{-17}$		
GAB2	0	EGA4	0.40 ± 0.01	$(10 \pm 6) \times 10^{-17}$		
	20	EGA4	0.41 ± 0.01	$(10 \pm 6) \times 10^{-17}$		
	40	EGA6	0.45 ± 0.02	$(4 \pm 2) \times 10^{-16}$		

[a] at $T = 300$ K for SIC, GA, GAE and at $T = 340$ K for GAB

annealing.

iv) The irradiation dose required to essentially change the parameters of the trap in the epitaxial structures was higher than one in single-crystal samples. In particular, table 1 provides data for the GAT (GAS) and GAB series samples after 20 s of MWT, which supports this fact. Notably, the doping levels of the GAB and GAE substrates were the same as those of samples GAS1 and GAT, and the doping level of the GAB epitaxial layer was similar to that of GAS2. In addition, GAB, GAE, and GAT contain the same doping impurities. Thus, the observed differences were determined by the sample's structures but not by the difference in their conductivities.

v) If t_{MWT} is not enough to change the level location, the MW-induced changes in the capture cross section are opposite for SiC single-crystal and GaAs epi-structures. In fact, σ_n were found to decrease in SIC1 and SIC2, while for GAE and GAB, the capture cross section increased.

We now consider the possible configurations of the defects detected in the structures under study. For this purpose, we should take into account that the reported data for the main trap parameters vary over a wide range; in particular, the difference between the values of capture cross sections can be as large as four orders of magnitude [30]. One of the possible reasons for such a large spread of parameters is the strong dependence of the charge thermal emission on the electric field strength [31, 32] caused by a) decrease in ionization energy due to the Pool–Frenkel effect or, for example, Coulombic interactions of defect [33] and b) change in the σ_n magnitude [34]. As a rule, the change in $(E_c - E_t)$ comprises several tens of meV, and the change in the capture cross-section reaches several orders of magnitude. For instance, according to Bourgoin and Angelis [34], at room temperature, σ_n for the $EL2$ center in GaAs decreases 200 times at an intensity of 10^5 V/cm. Consequently, the different methods used to investigate defects yield different parameters for the same centers. For example, from reviews on various traps in gallium arsenide, we can compare the data obtained by deep-level transient spectroscopy [35] and thermally stimulated currents [30]. Data were obtained for defects with closely located levels and very different capture cross section values. Generalizing the above-mentioned, we should note that it is the energy level that we shall be oriented towards in defect configuration determination. If the change in $(E_c - E_t)$ after MWT has exceeded the experimental errors limit (about 20 meV), we supposed the microwave-induced configuration change.

The position of the ESC1 level ($E_c - (0.33 - 0.34)$ eV) observed in the initial SiC crystals can be compared with the position of the S–center ($E_c -$ 0.35 eV) [36, 37, 38], EK–center ($E_c - 0.34$ eV) [39], or $(-/+)$ level $E1$ ($E_c - 0.34$ eV) [36]. S–center is responsible for non-radiative recombination, and in $6H$–SiC it is a self-interstitial defect [36]. According to the [37, 38], the S–center and R–center ($E_c - 1.27$ eV) are associated with two different charge states of the same defect, whereas according to Lebedev *et al*. [40], the R–center is a divacancy $V_{\mathrm{Si}}V_{\mathrm{C}}$. It should be noted that a divacancy is a typical defect in $6H$–SiC [41, 20]. On the other hand, the level $E_c - 0.39$ eV is more often associated with center $E1$ [21, 42]. Thus, in our opinion, ESC1 level is related to complex $V_{\mathrm{Si}}V_{\mathrm{C}}$.

After the MWT, the level of the trap, which is responsible for TAV arising in SiC, shifted to $E_c - (0.26 - 0.29)$ eV (level ESC2). This situation is also ambiguous: closely located are donor level $(0/+)$ of center $E1$ ($E_c - (0.27 - 0.28)$ eV [43], $E_c - 0.26$ eV [21, 42] and center $X1$ ($E_c - 0.3$ eV) [44]. The authors of the latter publication reported the essential dependence of $X1$ concentration on crystal structural perfection. They stressed that $X1$ was not identical to $E1$. In turn, level $E1$ has been identified as the center of the negative correlation energy [44, 21] and dominating intrinsic point defect in n–type $6H$–SiC [45]. According to Refs. [45, 21], $E1$ is related to carbon vacancy. Considering the difference between the $X1$ and ESC2 energy locations, the configuration V_{C} was associated with the ESC2 level. In addition, the connection between the level $E_c - 0.26$ eV and the carbon vacancy is confirmed by Grossner *et al* [46].

The data for levels revealed for gallium arsenide are listed in table 2. The presented data show that the traps are associated with intrinsic vacancy-related defects: EGA1 is V_{As}, EGA2 is $V_{\mathrm{As}}As_i$, EGA3 is V_{As} or $V_{\mathrm{Ga}}Ga_iV_{\mathrm{As}}$, EGA4 is $V_{\mathrm{Ga}}Ga_{\mathrm{As}}$, EGA5 is $V_{\mathrm{Ga}}V_{\mathrm{As}}$, and EGA6 is $V_{\mathrm{As}}As_i$.

Several factors caused the trap parameters to change. They are as follows.

i) Transformation of the defect complex due to decay, involvement of additional components, change in the distance between defect components, etc.

ii) Defect recharging.

iii) Changes in the trap environment, which can result, for instance, in the modified strength of the electric field around the defect.

iv) An increase in the concentration of a given type of defect; for instance, the change in ionization energy was reported [33] to be proportional to the cubic root of the defect concentration.

Analysis of the observed phenomena should consider the probable mechanisms of the impact of microwave radiation on the crystals. The primary process, which determines defect production under irradiation, is a displacement of the atoms from the sites of the lattice. But the energy of a

Table 2. Data reported for the levels close to detected levels

$(E_c - E_t)$, eV	σ_n, cm^2	configuration	method[a]	epi–structure	Reference
		EGA1, $(E_c - E_t) = (0.31 - 0.32)$ eV			
0.33	-	complex with V_{As}	DLTS	no	[47]
0.33	-	-	DLTS	no	[48]
$0.31 - 0.33$	-	V_{As}	LDA	no	[49]
0.33	1×10^{-17}	-	TSC	no	[30]
0.323	1×10^{-14}	-	DLTS	yes	[50]
0.334	2×10^{-15}		DLTS	yes	[50]
0.35	-	complex with V_{As}	PA	no	[51]
$0.315 - 0.325$	3×10^{-17}	-	TSC	no	[52]
0.33	-	-	TSC	no	[53]
$0.30 - 0.33$	-	-	DLTS	no	[54]
		EGA2, $(E_c - E_t) = (0.28 - 0.30)$ eV			
0.28	5×10^{-18}	$V_{As}As_i$	TSC	no	[30]
0.26	3.5×10^{-15}	-	DLTS	yes	[50]
0.30	-	intrinsic	DLTS	no	[55]
0.284	1×10^{-17}	-	TSC	no	[52]
0.28	-	intrinsic	TP	no	[56]
0.28	8×10^{-15}	-	DLTS	yes	[57]
0.30	-	complex with Te	DLTS	no	[58]
0.30	6×10^{-15}	$V_{As}As_i$	DLTS	no	[59]
		EGA3, $(E_c - E_t) = 0.49$ eV			
0.50	-	Sb_{Ga}	DLTS	no	[60]
0.48	4×10^{-16}	As_{Ga}^{++}	TSC	no	[30]
0.485	2×10^{-16}	-	TSC	no	[52]
0.48	-	impurity	TP	no	[56]
0.49	2×10^{-13}	impurity+V_{As}	DLTS	yes	[61]
0.48	3×10^{-13}	-	DLTS	no	[54]
0.50	1×10^{-15}	V_{As}, $V_{Ga}Ga_iV_{As}$	DLTS	no	[59]
		EGA4, $(E_c - E_t) = (0.39 - 0.41)$ eV			
0.42	-	-	DLTS	no	[48]
0.41	-	$V_{Ga}V_{As}$	DLTS	no	[60]
0.39	-	$V_{Ga}Ga_{As}$	TSC	no	[62]
0.41	2×10^{-13}	-	DLTS	yes	[35]
0.40	-	-	SCRC	yes	[63]
0.37	2×10^{-14}	-	DLTS	yes	[64]
0.40	-	$V_{Ga}Ga_{As}$	DLTS	no	[65]
0.387	2×10^{-14}	-	DLTS	yes	[50]
		EGA5, $(E_c - E_t) = (0.24 - 0.25)$ eV			
0.23	-	-	DLTS	no	[48]
0.23	2×10^{-17}	-	TSC	no	[30]
$0.22 - 0.25$	8×10^{-19}	-	TSC	no	[66]
0.26	-	complex with V_{Ga}	TSC	no	[62]
0.24	-	-	TSC	no	[53]
0.23	-	intrinsic	TP	no	[56]
0.23	-	$V_{Ga}V_{As}$	DLTS	no	[67]
0.23	1×10^{-14}	$V_{Ga}V_{As}$	DLTS	no	[35]
0.23	7×10^{-15}	-	DLTS	yes	[57]
0.236	1×10^{-16}	complex with V_{As}	DLTS	yes	[61]
0.258	4×10^{-16}	-	DLTS	yes	[50]
		EGA6, $(E_c - E_t) = (0.43 - 0.46)$ eV			
0.44	1×10^{-14}	$V_{As}As_i$, V_{As}	TSC	no	[30]
0.44	9×10^{-15}	-	TSC	no	[52]
0.43	7×10^{-16}	intrinsic	DLTS	yes	[68] [35]
0.44	2×10^{-15}	complex with V_{As}	DLTS	yes	[69]

[a] DLTS — deep level transient spectroscopy; TSC — thermally stimulated current; LDA — local density approximation; PA — positron annihilation techniques; TP — photoinduced transient spectroscopy; SCLC — space charge limited current

photon with frequency 2.45 GHz is about 10^{-5} eV only; the threshold displacement energies in GaAs and SiC are (8-28) eV [70] and (20-35) eV [71], respectively. Therefore such a channel of microwave-induced modification of defect subsystem is unreal.

Microwave energy is known to transform into heat inside the material. It is believed that the structural modification in the MWT result is mostly caused by the change in the defect charge state and elastic stress fields arising in instantly heated defect regions. Processes based on microwave heating find many industrial applications. But the used experimental procedure (pulsed microwave radiation with a period of 500 s and a duty cycle of 1%) allowed prevention of essential heating. The calculation according to Bacherikov *et al.* [17] shows that the maximum possible heating temperature of the sample ΔT is about 1 K. The ΔT magnitude was confirmed by measurements using a T–type thermocouple. Besides, the heating are known to intensify with increase in free charge carrier concentrations [6], whereas in our case, the revealed effects weaken with the concentration increase (samples GAS1 and GAS2). As a result, the influence of microwave heating can be neglected.

However, numerous studies have shown that the observed effects of MWT cannot be explained only by the mechanisms of fast annealing; therefore, non-thermal factors should also be considered [72, 73]. These phenomena can be related to various physical reasons. First, it is known [74, 75] that a free charged particle in an electromagnetic field performs a drift in parallel to the electric component. The drift velocity magnitude is given by $v_\perp \propto (E_0/m\nu)$ (where E_0 is the amplitude of the electric field, m is the mass of the particle) and velocity direction depends on the phase of the field at the initial time. Consequently, along with the systematic drift of individual charged particles, directional movement of the entire set of particles is absent. Besides, the particle drifts in the direction of wave propagation with the velocity $v_\parallel \propto (E_0/m\nu)^2$. However, the charged point defects in semiconductor crystal are not free and have to overcome potential barriers when moving. It can be taken into account by using effective mass m_{eff}, which exponentially depends on barrier height [75]. In our opinion, the mentioned features testify that such MW-induced movement is not responsible for revealed effects.

Second, the ponderomotive forces can arise under MW action. Under inhomogeneous microwave electromagnetic field conditions, the induced oscillatory defect fluxes are rectified, leading to directional, macroscopic mass transport [73, 76, 77]. The ponderomotive force can be described as follows [76, 75]:

$$F_p(x) = \frac{q^2 \beta E_0^2}{8 m_{\text{eff}} \pi^2 \nu^2} \exp(-2\beta x), \qquad (3)$$

where q is the charge of the defect, and β is the coefficient of electromagnetic wave absorption, the axis x is along the direction of wave propagation. On the one hand, the both the MW attenuation and ponderomotive force are essential when $d \geq \beta^{-1}$ (where d is the thickness of the semiconductor crystal). On the other hand, the following expression can be used to estimate β [75]:

$$\beta = \frac{1}{c} \left(\frac{\sigma \pi \nu}{\varepsilon_0} \right)^{\frac{1}{2}}, \qquad (4)$$

where $\sigma = e n \mu_n$ is crystal conductivity; μ_n is the electron mobility, 8500 cm^2/sV for GaAs, 400 cm^2/sV for SiC. Accordind to [75], the equation (4) is correct in the case of $(\sigma/2\pi\varepsilon_0\varepsilon\nu) \gg 1$ (where ε is the dielectric perminity; 12.9 for GaAs, 10.03 for SiC), which corresponds to the samples under investigation. The calculations show that β^{-1} is $(57 - 90)$ μm for SiC crystals, 138 μm for GAS2, 20 μm for GAS1 and substrate of epitaxial structures, $(100 - 470)$ μm for epi-layers. Thus the ponderomotive forces are able to cause the movement of the charged point defects both in the single-crystal samples and substrate of epitaxial structures, and the effect is maximal in the near–surface region. Though ponderomotive influence can not be the only reason for observed effects. In fact $\beta(\text{GAS1}) > \beta(\text{GAS2})$, however, MWT with $t_{\text{MWT}} = 20$ s does not lead to defect transformation in GAS1, unlike in GAS1 — see table 1. Similar results are observed for SIC1(2) and SIC3.

Third, it was shown [78, 79, 80] that under resonance conditions (the coincidence of eigenfrequencies of the dislocation segment vibrations and electrical component of the microwave radiation), multiple dislocation loops occur. Besides, the MWT causes the movement of dislocations. In particular, at $\nu = 2.45$ GHz for GaAs, resonant detachment of numerous dislocations with the length $L \leq 4$ μm becomes possible [80]. The dislocation climb is accompanied by intrinsic defect generation. In addition, the behavior of the dislocation segment in a MW electric field may be strongly affected by impurity atoms, which decorate dislocations. Having accumulated at dislocations, they, on the one hand, decrease resonance frequency; on the other hand, impurity atoms may detach from dislocations at high oscillation amplitudes, and free impurity atoms may appear in the crystal [78, 79]. In turn, the appearance of free doping atoms can result in an intrinsic defect concentration increase. In our case, the dislocation generation is confirmed by a change in both curvature radius and deformation of the near-surface crystallographic planes after MWT.

Fourth, the MW-induced destruction of impurity complexes, united in clusters, is described [78, 79, 80]. This is resonant phenomenon as well, and it is expected if the irradiation frequency is close to

ion–plasma frequency $\nu_r = \sqrt{e^2 N_{\text{com}}/4\pi^2 \varepsilon_0 \varepsilon \mu}$ (where N_{com} is the complex concentration in the cluster, μ is the reduced mass of complex ions). For example, ν_r equals to 2.01 GHz for Te$^+$–Cu$^-$ complex with $N_{\text{com}} = 5 \cdot 10^{16}$ cm^{-3} in GaAs [78]. But since the revealed transformation of deep levels relates to intrinsic defects, this mechanism seems unlikely. Besides, data about defect clusters in the samples under investigation are absent.

The observed modifications of deep-level parameters are the result of the above-mentioned structural reconstruction in semiconductor near-surface regions owing to the MWT. The results of X–ray investigations show that MWT increases the convexity of single-crystal samples, which indicates the aggregation of interstitial defects in the near-surface layer, particularly because of the generation of separate dislocations [11, 19]. The defect accumulation effect caused by the MWT in the near-surface region was reported in [11, 18]. To a certain extent, only the SIC3 sample was excluded; however in this case, a rather strong deformation of the near-surface region was also observed prior to irradiation. Researchers have reported [9, 10, 11, 12, 13] that in this stressed state, MWT causes redistribution as well as certain weakening of elastic deformations, which is what occurs in SIC3. The profilometry data correlated with X–ray measurements. Structural investigations show that in the initial GaAs samples, the density of dislocations has a W-like distribution over the plate area; the dislocation density over the plate diameter varied from $2 \cdot 10^4$ cm^{-2} to $2 \cdot 10^5$ cm^{-2}. This inhomogeneity in the dislocation density distribution is evidence of considerably strong elastic deformation in the sample.

In our opinion, the process of MWT influence was two-stage. Initially, the resonant movement of the dislocation segment has caused an increase in the concentration of point defects, which are mostly intrinsic interstitial atoms. The approach of primary vacancy-related defects and secondary defects under the ponderomotive forces action and subsequent defect reactions occurred at the final stage. If the time of MW processing is not long enough for an essential increase in interstitial atom concentration or effective mass transport, the defect transformation does not occur, and the energy level does not change. In this case, the modification of electron capture cross-section is able under a field of newly formed dislocations (or distant point defects).
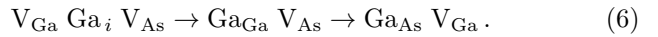
For example, let's consider a microwave influence on silicon carbide. MWT with $t_{\text{MWT}} = 20$ s leads to a decrease in σ_n magnitude for ESC1 (V$_{\text{Si}}$V$_{\text{C}}$) in SIC1 and SIC2. The further irradiation causes the trap modification, and the ESC1 center transforms into ESC2 (V$_{\text{C}}$) under the influence of closely located interstitial silicon:

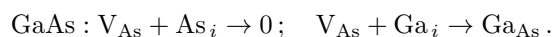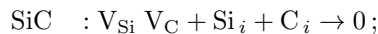$$\text{V}_{\text{Si}}\,\text{V}_{\text{C}} + \text{Si}_i \to \text{V}_{\text{C}}\,.$$
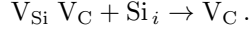
In the case of SIC3 sample, the defect transformation occurred at a low dose because MW-induced effects are enhanced by intensive lattice strain. In fact, the deformation of the near-surface crystallographic planes in SIC3 is significant compared with SIC1 and SIC2 ones — see table 1. Further MW-induced modification of the ESC2 parameters in SIC3 is caused by the enhanced electric field of the newly formed dislocation.

Similar processes occur in a GaAs single-crystal. The transformations EGA1→EGA2 (GAS2 sample) and EGA3→EGA4 (GAT sample), which because of the increased number of interstitial atoms in the near-surface layer, can be described by using the following reaction:

$$\text{V}_{\text{As}} + \text{As}_i \to \text{V}_{\text{As}}\,\text{As}_i\,; \tag{5}$$

$$\text{V}_{\text{Ga}}\,\text{Ga}_i\,\text{V}_{\text{As}} \to \text{Ga}_{\text{Ga}}\,\text{V}_{\text{As}} \to \text{Ga}_{\text{As}}\,\text{V}_{\text{Ga}}\,. \tag{6}$$

It should be noted that the reaction (6) is proposed by Fang *et al* [62]. The cause of the weak (in comparison with GAS2) MWT influence on the trap in the initial GAS1 sample is the absence of pressure stresses $(\xi_{\text{cur}}(t_{\text{MWT}} = 0) < 0)$, which intensify the MWT-stimulated complex formation process in the crystal's intrinsic defects. This is supported by data for silicon carbide single-crystals. Additionally, the GAS1 has a higher charge carrier concentration. It has been reported [7] that with a growth in resistance, the depth of microwave penetration increases, and thus, the volume from which defect gettering begins in the near-surface layer grows as well. On the other hand, the weaker efficiency of MWT influence in the sample with low electron concentration testifies that the ponderomotive forces are not the primary reason for the defect transformation. The GAT and GAB samples are differently doped: tin and tellurium atoms are predominantly located at the gallium and arsenic lattice sites, respectively. In our opinion, it is a minor reason for the difference in the initial defect structure of samples and MWT features. The root reason is connected to the different crystallin orientation of wafers.
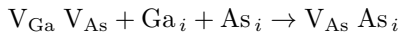
Accumulation of a large number of interstitial atoms in the near-surface layer at high doses ($t_{\text{MWT}} \approx$ 40 s for gallium arsenide and $t_{\text{MWT}} > 80$ s for silicon carbide) causes complete annihilation of vacancies (or transformation into antisite defects, whose levels are filled in the crystals with electron conductivity and cannot take part in acousto-electric interaction). Therefore, the TAV signal disappears (samples GAS1, GAS2, SIC1):

$$\text{SiC} \quad : \text{V}_{\text{Si}}\,\text{V}_{\text{C}} + \text{Si}_i + \text{C}_i \to 0\,;$$

$$\text{GaAs} : \text{V}_{\text{As}} + \text{As}_i \to 0\,; \quad \text{V}_{\text{As}} + \text{Ga}_i \to \text{Ga}_{\text{As}}\,.$$
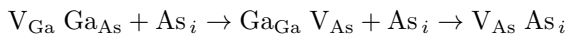
At the same time, the high density of dislocation at the near-surface layer should obstruct the MW-induced point defect reactions. Really, the extended defects can precipitate newly formed interstitial atoms and thus prevent vacancy transformation. We hypothesize that the microwave hardness of the trap in SIC3 is associated with the detected deformations of the near-surface crystallographic planes.

It is believed [27, 25, 24] that the TAV that arises in epitaxial structures is mostly caused by defects located at the epi–layer and substrate interface. In addition, the growth of epitaxial layers is known to lead to the arising of redundant dislocations at the interface. There are two reasons which cause the difference between the dose-dependent modification of the defect in the epitaxial and single-crystal samples.

It was reported [11, 19] that the MWT induced increase in curvature radius in epitaxial structures n–n^+–GaAs and n–n^+–n^{++}–GaAs. This phenomenon deals with forming single dislocations and their further propagation deep into the structure along the glide planes [11, 19]. In our case, the defect transformation was the outcome. As shown in table 2, EGA5 and EGA6 levels were associated with the complexes $V_{Ga}V_{As}$ and $V_{As}As_i$, respectively. Traps such as EGA2 and EGA4 have also been previously found in epi-structures [50, 57, 35, 63, 64, 68, 69]. The detected MW-stimulated reactions, which are caused by an increasing number of interstitial atoms, can be described as follows:

$$V_{Ga}\,V_{As} + Ga_i + As_i \rightarrow V_{As}\,As_i$$

for GAE1 and GAE2, and

$$V_{Ga}\,Ga_{As} + As_i \rightarrow Ga_{Ga}\,V_{As} + As_i \rightarrow V_{As}\,As_i$$

for GAB1 and GAB2. EGA6 corresponds to the final defect configuration in GAE1 and GAE2 samples. Thus the increase in EGA6 activation energy in sample GAE3 is probably caused by the change in Coulombic interaction of interstitial–vacancy complexes, which is due to a variation in their concentration. The similar effect of the change in ionization energy was reported previously [33]. The increase in capture cross section of EGA4 (GAB1, $t_{MWT} = 20$ s) and EGA6 (GAE3) are associated with the growth of the electric field strength caused by charged dislocations.

4. Conclusion

The influence of microwave radiation on the parameters of point defects (cross section of electron capture and energy levels in the gap) was studied experimentally in single crystals of n–$6H$-SiC and n–GaAs, as well as in gallium arsenide epitaxial structures. The investigation showed that the traps available in the near-surface layer are associated with intrinsic vacancy-related defects. The microwave-induced change in the trap energy level and capture cross section was caused by the growing number of interstitial atoms in the near-surface layer. The possible defect reactions have been discussed. The radiation-stimulated process involving the transformation of defect complexes intensifies under stress conditions. Thus microwave processing can be an effective tool of defect engineering.

Data Availability Statement

The data that support the findings of this study are available from the corresponding author upon reasonable request.

References

[1] Kozlovskii V V, Kozlov V A and Lomasov V N 2000 *Semiconductors* **34**(2) 123–140
[2] Schrimpf R D and Fleetwood D M 2004 *Radiation Effects and Soft Errors in Integrated Circuits and Electronic Devices* (World Scientific) ISBN 981-238-940-7
[3] Kabiraj D and Ghosh S 2011 *J. Appl. Phys.* **109** 033701
[4] Olikh O Y, Gorb A M, Chupryna R G and Pristay-Fenenkov O V 2018 *J. Appl. Phys.* **123** 161573
[5] Olikh O and Pinchuk T 2006 *Tech. Phys. Lett.* **32** 517–519
[6] Kitchen H J, Vallance S R, Kennedy J L, Tapia-Ruiz N, Carassiti L, Harrison A, Whittaker A G, Drysdale T D, Kingman S W and Gregory D H 2014 *Chem. Rev.* **114** 1170–1206
[7] Zohm H, Kasper E, Mehringer P and Müller G 2000 *Microelectron. Eng.* **54** 247–253
[8] Bhunia S and Bose D 1998 *J. Cryst. Growth* **186** 535–542
[9] Bacherikov Y Y, Konakova R V, Kocherov A N, Lytvyn P M, Lytvyn O S, Okhrimenko O B and Svetlichnyi A M 2003 *Technical Physics* **48**(5) 598–601
[10] Pashkov V, Perevoshchikov V and Skupov V 1994 *Pis'ma v zhurnal tekhnicheskoy fiziki* **20**(8) 14–18 (in Russian)
[11] Boltovets N S, Kamalov A B, Kolyadina E Y, Konakova R V, Lytvyn P M, Lytvyn O S, Matveeva L A, Milenin V V and Rengevych O E 2002 *Technical Physics Letters* **28**(2) 154–156
[12] Milenin V, Konakova R, Statov V, Sklyarevich V, Tkhorik Y, Filatov M and Shevelev M 1994 *Pis'ma v zhurnal tekhnicheskoy fiziki* **20**(4) 32–36 (in Russian)
[13] Belyaev A, Venger E, Ermolovich I, Konakova R, Lytvyn P, Milenin V, Prokopenko I, Svechnikov G, Soloviev E and Fedorenko L 2002 *Effect of microwave and laser radiations on the parameters of semiconductor structures* (Kyiv: Intac)
[14] Ashkinadze B, Cohen E, Ron A, Linder E and Pfeiffer L 1996 *Solid-State Electron.* **40** 561–565 ISSN 0038-1101
[15] Ermolovich I B, Venger E F, Konakova R V, Milenin V V, Svechnikov S V and Sheveljev M V 1998 *Proc. SPIE* **3359** 265–272
[16] Belyayev A, Belyayev A, Yermolovich I, Komirenko S, Konakova R, Lyapin V, Milenin V, Solov'ev E and Shevelev M 1998 *Technical Physics* **43** 1445–1449
[17] Bacherikov Y, Konakova R, Milenin V, Okhrimenko O, Svetlichnyi A and Polyakov V 2008 *Semiconductors* **42**(7) 868–872
[18] Zayats N S, Konakova R V, Milenin V V, Milenin G V, Red'ko R A and Red'ko S N 2015 *Technical Physics* **60**(3) 432–436
[19] Belyaev A, Sachenko A, Boltovets N, Ivanov V, Konakova R, Kudryk Y, Matveeva L, Milenin V, Novitskii S and Sheremet V 2012 *Semiconductors* **46**(4) 541–544

[20] Davidsson J, Ivády V, Armiento R, Ohshima T, Son N T, Gali A and Abrikosov I A 2019 *Appl Phys Lett* **114** 112107

[21] Wei Y, Tarekegne A T and Ou H 2018 *J. Appl. Phys.* **124** 054901

[22] Pellegrino C, Gagliardi A and Zimmermann C G 2020 *J. Appl. Phys.* **128** 195701

[23] Sobolev M M, Soldatenkov F Y and Danil'chenko V G 2020 *J. Appl. Phys.* **128** 095705

[24] Ostrovskii I V, Saiko S V and Walther H G 1998 *J. Phys. D: Appl. Phys.* **31** 2319–2325

[25] Ostrovskii I and Olikh O 1998 *Solid State Commun.* **107** 341–343

[26] Gromashevskii V, Tatyanenko N and Snopok B 2013 *Semiconductors* **47**(4) 579–585

[27] Abbate A, Ostrovskii I V, Han K J, Masini G, Palma F and Das P 1995 *Semicond. Sci. Technol.* **10** 965–969

[28] Jamnický I and Bury P 1993 *physica status solidi (a)* **139** K35–K38

[29] Godwod K, Nagy A T and Rek Z 1976 *Phys. Status Solidi A* **34** 705–710

[30] Pavlović M, Desnica U V and Gladić J 2000 *J. Appl. Phys.* **88** 4563–4570

[31] Bulyarskii S, Grushko N and Zhukov A 2000 *Semiconductors* **34**(1) 40–44

[32] Makram-Ebeid S and Lannoo M 1982 *Phys. Rev. B* **25**(10) 6406–6424

[33] Stellmacher M, Bisaro R, Galtier P, Nagle J, Khirouni K and Bourgoin J C 2001 *Semicond. Sci. Technol.* **16** 440–446

[34] Bourgoin J C and De Angelis N 2001 *Semicond. Sci. Technol.* **16** 497–501

[35] Bourgoin J C, von Bardeleben H J and Stiévenard D 1988 *J. Appl. Phys.* **64** R65–R92

[36] Lebedev A A 1999 *Semiconductors* **33**(2) 107–130

[37] Anikin M, Andreyev A, Lebedev A, Pyatko S, Rastegayeva M, Savkina N, Strel'chuk A, Syrkin A and Chelnokov V 1991 *Fizika i tekhnika poluprovodnikov* **25**(2) 328–333 (in Russian)

[38] Anikin M, Zubrilov A, Lebedev A, Strel'chuk A and Cherenkov A 1991 *Fizika i tekhnika poluprovodnikov* **25**(3) 479–486 (in Russian)

[39] Kuznetsov N and Edmond J 1997 *Semiconductors* **31**(10) 1049–1052

[40] Lebedev A, Veinger A, Davydov D, Kozlovskii V, Savkina N and Strel'chuk A 2000 *Semiconductors* **34**(8) 861–866

[41] Baranov P G, Il'in I V, Mokhov E N, Muzafarova M V, Orlinskii S B and Schmidt J 2005 *Journal of Experimental and Theoretical Physics Letters* **82** 441–443

[42] Koizumi A, Markevich V P, Iwamoto N, Sasaki S, Ohshima T, Kojima K, Kimoto T, Uchida K, Nozaki S, Hamilton B and Peaker A R 2013 *Appl. Phys. Lett.* **102** 032104

[43] Hemmingsson C G, Son N T and Janzén E 1999 *Appl. Phys. Lett.* **74** 839–841

[44] Lebedev A, Davydov D, Tregubova A, Bogdanova E, Shcheglov M and Pavlenko M 2001 *Semiconductors* **35**(12) 1372–1374

[45] Sasaki S, Kawahara K, Feng G, Alfieri G and Kimoto T 2011 *J. Appl. Phys.* **109** 013705

[46] Grossner U, Grillenberger J K, Woerle J, Bathen M E and Müting J 2021 *Intrinsic and Extrinsic Electrically Active Point Defects in SiC* (John Wiley & Sons, Ltd) chap 6, pp 137–168

[47] Richter T, Kühnel G, Siegel W and Niklas J R 2000 *Semicond. Sci. Technol.* **15** 1039–1044

[48] Neild S T, Skowronski M and Lagowski J 1991 *Appl. Phys. Lett.* **58** 859–861

[49] Schultz P A 2015 *J. Phys.: Condens. Matter* **27** 075801

[50] Yousefi G H, Webb J B, Rousina R and Khanna S M 1995 *J. Electron. Mater.* **24** 15–20

[51] Kuisma S, Saarinen K, Hautojärvi P, Fang Z Q and Look D 1997 *J. Appl. Phys.* **81** 3512–3521

[52] Pavlović M and Desnica U V 1998 *J. Appl. Phys.* **84** 2018–2024

[53] Tomozane M and Nannichi Y 1986 *Japanese Journal of Applied Physics* **25** L273–L275

[54] Lang D V, Cho A Y, Gossard A C, Ilegems M and Wiegmann W 1976 *J. Appl. Phys.* **47** 2558–2564

[55] Stievenard D, Boddaert X and Bourgoin J C 1986 *Phys. Rev. B* **34**(6) 4048–4058

[56] Abele J C, Kremer R E and Blakemore J S 1987 *J. Appl. Phys.* **62** 2432–2438

[57] Mircea A and Mitonneau A 1975 *Applied physics* **8** 15–21

[58] Kol'chenko T and Lomako V 1994 *Fizika i tekhnika poluprovodnikov* **28**(5) 857–860 (in Russian)

[59] Pons D and Bourgoin J C 1985 *J. Phys. C: Solid State Phys.* **18** 3839–3871

[60] Samoylov V A, Yakusheva N A and Prints V Y 1994 *Fizika i tekhnika poluprovodnikov* **28**(9) 1617–1626 (in Russian)

[61] Blood P and Harris J J 1984 *J. Appl. Phys.* **56** 993–1007

[62] Fang Z, Shan L, Schlesinger T and Milnes A 1990 *Materials Science and Engineering: B* **5** 397–408

[63] Ashby A, Roberts G, Ashen D and Mullin J 1976 *Solid State Commun.* **20** 61–63

[64] Fang Z Q, Schlesinger T E and Milnes A G 1987 *J. Appl. Phys.* **61** 5047–5050

[65] Vaytkus Y, Storasta Y, Pintsevichyus A, Pyatrauskas M and Kazhukauskas V 1988 *Litovskiy fizicheskiy sbornik* **28**(6) 744–751 (in Russian)

[66] Lin A L, Omelianovski E and Bube R H 1976 *J. Appl. Phys.* **47** 1852–1858

[67] Morrow R A 1991 *J. Appl. Phys.* **69** 3396–3398

[68] Lefèvre H and Schulz M 1977 *Applied physics* **12** 45–53

[69] Kol'chenko T, Lomako V, Rodionov A and Sveshnikov Y 1989 *Fizika i tekhnika poluprovodnikov* **23**(4) 626–629 (in Russian)

[70] Chen N, Gray S, Hernandez-Rivera E, Huang D, LeVan P D and Gao F 2017 *J Mater Res* **32** 1555–1562

[71] Debelle A, Thomé L, Dompoint D, Boulle A, Garrido F, Jagielski J and Chaussende D 2010 *J. Phys. D: Appl. Phys.* **43** 455408

[72] Nozariasbmarz A, Dsouza K and Vashaee D 2018 *Appl. Phys. Lett.* **112** 093103

[73] Bykov Y V, Rybakov K I and Semenov V E 2001 *J. Phys. D: Appl. Phys.* **34** R55–R75

[74] Bolotovskiĭ B M and Serov A V 2003 *Phys.-Uspekhi* **46** 645–655

[75] Milenin G V and Red'ko R A 2020 *Semiconductor Physics, Quantum Electronics & Optoelectronics* **23** 46–51

[76] Rybakov K I, Semenov V E, Freeman S A, Booske J H and Cooper R F 1997 *Phys. Rev. B* **55**(6) 3559–3567

[77] Rybakov K I and Semenov V E 1995 *Phys. Rev. B* **52**(5) 3030–3033

[78] Red'ko R, Milenin G and Milenin V 2017 *J Lumin* **192** 1295–1299

[79] Ermolovich I, Milenin G, Milenin V, Konakova R and Red'ko R 2007 *Technical Physics* **77**(9) 1173–1177

[80] Milenin G V and Red'ko R A 2019 *Semiconductor Physics, Quantum Electronics & Optoelectronics* **22** 39–46